nature materials

SUPPLEMENTARY INFORMATION

https://doi.org/10.1038/s41563-018-0063-z

In the format provided by the authors and unedited.

Highly reversible zinc metal anode for aqueous batteries

Fei Wang[1,2], Oleg Borodin[2], Tao Gao[1], Xiulin Fan[1], Wei Sun[1], Fudong Han[1], Antonio Faraone[3], Joseph A Dura[3], Kang Xu[2*] and Chunsheng Wang[1*]

[1]Department of Chemical and Biomolecular Engineering, University of Maryland, College Park, MD, USA. [2]Electrochemistry Branch, Sensor and Electron Devices Directorate, Power and Energy Division, US Army Research Laboratory, Adelphi, MD, USA. [3]NIST Center for Neutron Research, National Institute of Standards and Technology, Gaithersburg MD, USA. *e-mail: conrad.k.xu.civ@mail.mil; cswang@umd.edu

Supplementary Information

Highly Reversible Zinc Metal Anode for Aqueous Batteries

Fei Wang,[a,b] Oleg Borodin, [b] Tao Gao,[a] Xiulin Fan,[a] Wei Sun, [a] Fudong Han,[a] Antonio Faraone,[c] Joseph A Dura,[c] Kang Xu [b] and Chunsheng Wang* [a]*

a. Department of Chemical and Biomolecular Engineering, University of Maryland, College Park , MD 20742 , USA
b. Electrochemistry Branch, Sensor and Electron Devices Directorate, Power and Energy Division, U.S. Army Research Laboratory, Adelphi, MD 20783, USA.
c. NIST Center for Neutron Research, National Institute of Standards and Technology, Gaithersburg, MD20899, USA

Supplementary Notes

Molecular Dynamics Studies of Aqueous Electrolytes doped with LiTFSI and $Zn(TFSI)_2$

Molecular dynamics (MD) simulations were performed on aqueous electrolytes doped with 1m $Zn(TFSI)_2$ and three concentrations of LiTFSI salts 5m, 10m and 20m as a function of temperature. The simulation cell contained 9 $Zn(TFSI)_2$, 92 LiTFSI and 1024 water for the 5m LiTFSI + 1m $Zn(TFSI)_2$ electrolyte; 18 $Zn(TFSI)_2$, 184 LiTFSI and 1024 water for the 10 m LiTFSI + 1m $Zn(TFSI)_2$ electrolyte; and 9 $Zn(TFSI)_2$, 174 LiTFSI and 484 water for the 20 m LiTFSI + 1m $Zn(TFSI)_2$ electrolyte. The previously developed many-body polarizable force field (APPLE&P) for LiTFSI – H_2O was used as a basis for the developed force field.[24] The $Zn^{2+}/TFSI^-$ and Zn^{2+}/H_2O repulsion interactions were fit to reproduce binding energies of the $Zn^{2+}(H_2O)_n$ and $Zn^{2+}(TFSI^-)_m$ clusters with n=1,4,6 and m=1,2,3 in gas-phase as shown in Table S1. Optimized complex geometries from DFT and molecular mechanics using developed force field are shown in Figures S5 and S6, respectively, demonstrating that the force field adequately describes both energetics and geometries of the Zn-based solvates. The force field functional form, combining rules and development methodology are described elsewhere.[1]

Table S1. Binding energy (in kcal/mol) of the $Zn^{2+}(H_2O)_n$ and $Zn^{2+}(TFSI^-)_m$ clusters with n=1,4,6 and m=1,2,3 in gas-phase from M05-2X/6-311+G(2d2f) DFT calculations and developed force field (FF)

complex	DFT	FF	Geometry from Fig. S5-S6
Zn/TFSI (C_2)	-364.5	-364.5	a
Zn/TFSI (C_1)	-363.9	-363.8	b
Zn/TFSI (C_2)	-346.0	-345.4	c
$Zn/(TFSI)_2$	-539.2	-537.7	d
$Zn/(TFSI)_3$	-589.6	-597.6	e
$Zn(H_2O)_6$	-359.3	-359.3	
$Zn(H_2O)_4$	-297.7	-321.7	
$Zn(H_2O)$	-100.9	-113.5	

Due to much stronger binding of the Zn^{2+} cation to water and $TFSI^-$ compared to the Li^+ cation

binding to the $TFSI^-$ anion and water, the anion and solvent (water) exchange in the first coordination shell of Zn^{2+} is significantly (two orders of magnitude) slower compared to the relaxation of the Li^+ cation first coordination shell. Because of the slower relaxation we estimate that MD simulation runs longer than 1000 ns (1μs) are required in order to obtain the equilibrium Zn^{2+} coordination shell structure at room temperature for the highly concentrated electrolytes. Such calculations are too computationally expensive for the available resources. Instead, we performed MD simulations as a function of temperature at 363 K, 393 K and 450 K (overheated system) and extrapolated solvation behavior to room temperature. Due to higher thermal fluctuations at higher temperature, relaxation in the Zn^{2+} solvates is significantly faster at higher temperature and results for the Zn^{2+} coordination are adequately converged at 393 K and 450 K. Multiple systems with different initial configurations were set up in order to ensure that final coordination does not depend on the initial conditions. Figure S7 shows evolution of the Zn^{2+} coordination shell during MD simulations. At 450 K it took on the order of 15-20 ns for the Zn^{2+} coordination to change from $Zn(H_2O)_6$ to Zn^{2+} coordinated by 5-6 oxygen atoms of $TFSI^-$ for 10m LiTFSI and 20m LiTFSI + 1m $Zn(TFSI)_2$ electrolytes. At 393 K, the Zn^{2+} coordination shell equilibrated on the time scale of 100 ns.

Understanding of Zn Coordination using Density Functional Theory

The Zn^{2+} hydration free energy was calculated for the $Zn(H_2O)_n$ clusters and shown in Table S2. As the number of water molecules explicitly included in the Zn^{2+} solvation shell systematically increased from two to six, the calculated free energy of hydration decreased and converge to around -464 kcal/mol. These results are in between the quasi-experimental value of -471.1 kcal/mol and the previous estimate from DFT calculations of -458.1 kcal/mol that utilized B3LYP hybrid density functional,[2] suggesting that M05-2X/6-311+G(2d,2p) calculations are sufficiently accurate for predicting Zn-water binding energies. Experimental evidence also indicated that Zn^{2+} is coordinated by six waters. [3] Table S2 shows that when the Zn^{2+} cation coordination shell explicitly contains only one or two water molecules, the free energy of hydration is about 15 kcal/mol larger than when all six water molecules in the Zn^{2+} first coordination shell are explicitly considered. Thus, it is important to include all water molecules in the first coordination shell of Zn^{2+} to accurately predict solvation energies.

Table S2. The hydration free energy at 298 K (ΔG^{hydr}) from M05-2X/6-311+G(2d,2p) DFT calculations with SMD(water) solvation model.

	ΔG^{hydr} (kcal/mol)
$Zn(H_2O)$	-480
$Zn(H_2O)_2$	-482
$Zn(H_2O)_4$	-477
$Zn(H_2O)_5(H_2O)$	-465
$Zn(H_2O)_6$	-464

Next we examined the $ZnTFSI(H_2O)_4$ clusters immersed in implicit solvent as shown in Figure S8. The clusters were setup with the Zn^{2+} cation coordinating one or two $TFSI^-$ oxygen atoms. During geometry optimization, however, the Zn^{2+} cation become coordinated only by water molecules with the $TFSI^-$ anions being pushed to the second coordination shell. These calculations indicate the propensity of Zn-TFSI to dissociate when a sufficient number of water molecules is present to completely hydrate the Zn^{2+} cation.

In order to further examine the preference of Zn^{2+} to be coordinated by water and $TFSI^-$ anions in dilute solutions, the free energy of $Zn(TFSI)_3$ and $Zn(TFSI)_2(H_2O)_2$ complexes in implicit water was calculated relative to the $Zn(H_2O)_6$ solvate and other isolated species in implicit water. Table S3 shows that the Zn – TFSI aggregates are less energetically favorable than $Zn(H_2O)_6$ and a dissociated $TFSI^-$ anion surrounded by water because of the positive sign of the relative free energy for the $Zn(TFSI)_3$ and $Zn(TFSI)_2(H_2O)_2$ complexes.

Table S3. Free energy (ΔG) of complexes in implicit solvent SMD(water) relative to $Zn(H_2O)_6$.

Complex	ΔG (kcal/mol)
$Zn(H_2O)_6$	0.0
$Zn(H_2O)_5(H_2O)$	-0.8
$Zn(TFSI)_3$ (a)	3.1
$Zn(TFSI)_3$ (b)	2.4
$Zn(TFSI)_2(H_2O)_2$	0.7

The reduction potentials were calculated using DFT for the representative $Zn(TFSI)_m(H_2O)_n$ complexes surrounded by implicit solvent as shown in Figure S9. The reduction potential of complex A was calculated as the negative of the free energy of formation of A^- in solution [$\Delta G^S_{298}=G^S_{298}(A^-) - G^S_{298}(A)$] divided by Faraday's constant as given by:

$$E_{red} = -\frac{\Delta G^S_{298K}}{F} - 1.4\ V, \quad (1)$$

The difference between the Li^+/Li scale and absolute reduction potential of 1.4 V was subtracted to convert DFT results to the Li^+/Li scale as discussed extensively elsewhere.[4]

When water was in direct contact with the Zn^{2+} cation in the $Zn(TFSI)_2(H_2O)_2$ or $Zn(H_2O)_6$ solvates, H_2 evolution reaction occurred at higher potentials than for the $TFSI^-$ anion decomposition by S-C bond braking. Reduction of $Zn(TFSI)_2$ cluster accomponized by the Zn-F bond formation was found to be around 1.66 V vs. Li/Li^+. The reduction potential for the $Li^+_2(TFSI^-)$ clusters in implicit water was previously shown to be 2.6-2.9 V vs. Li/Li^+,[1] which is higher than the reduction potential for the H_2 evolution, thus in highly concentrated LiTFSI solutions SEI formation is expected to form at higher potentials compared to H_2 evolution and zincate formation.

Supplementary Figures

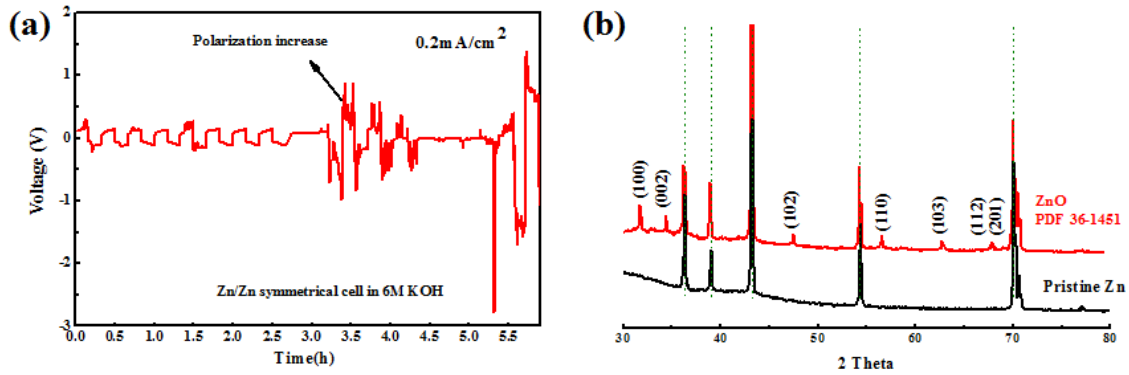

Figure S1. (a) Zn stripping/plating from Zn/Zn symmetrical cells at 0.2 mA/cm^2 in a 6 M KOH alkaline electrolyte. (b) XRD spectrum of a Zn anode after 100 cycles in the 6 M KOH alkaline electrolyte.

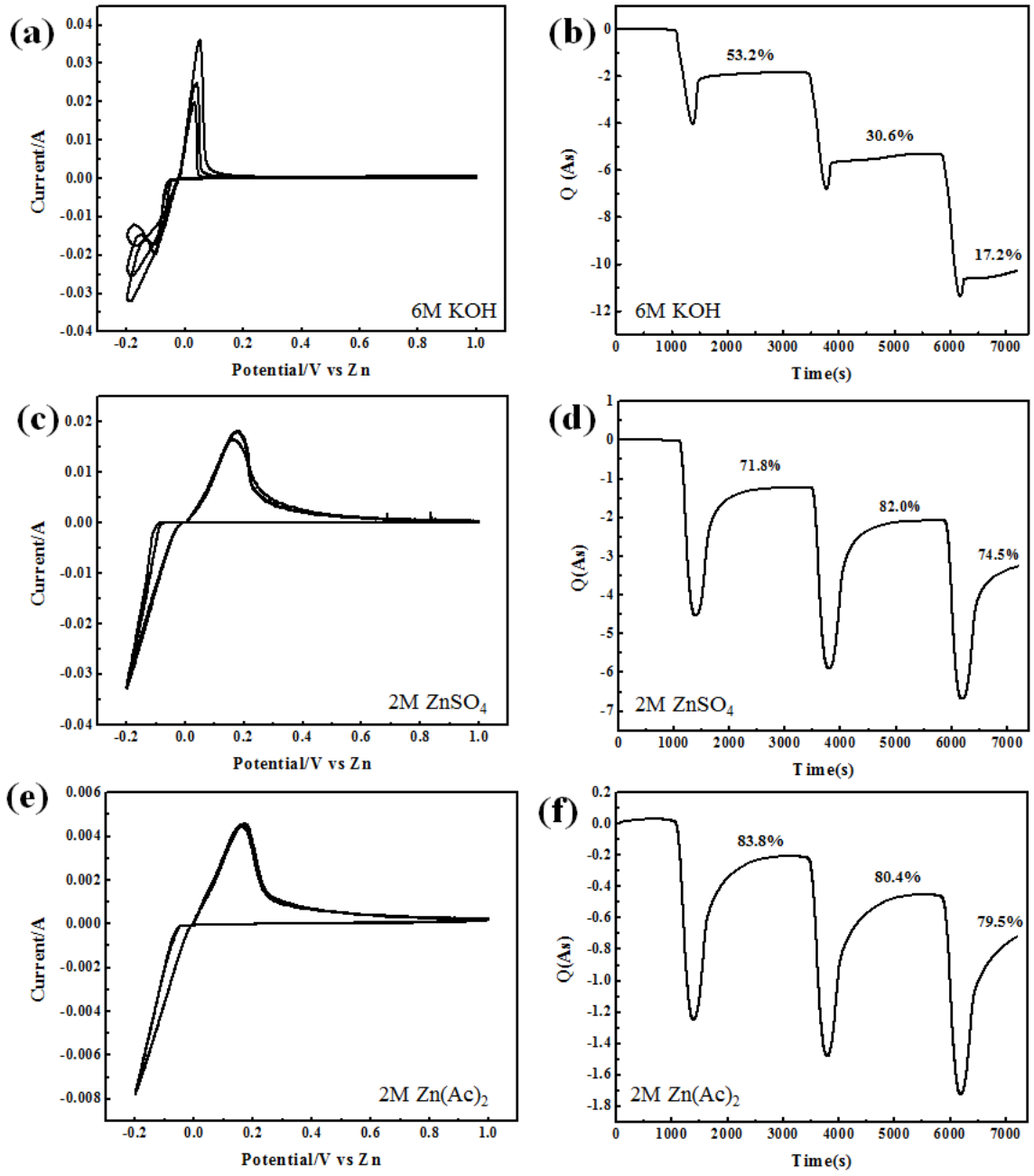

Figure S2. The cyclic voltammogram (CV) of Zn plating/stripping in a three-electrode cell using a Pt as a working electrode and a Zn metal as reference and counter electrode in the (a) 6 M KOH alkaline, (c) 2 M $ZnSO_4$ and (e) 2 M $Zn(Ac)_2$ electrolytes and the columbic effiency of Zn metal plating/stripping in the (b) 6 M KOH alkaline, (d) 2 M $ZnSO_4$ and (f) 2 M $Zn(Ac)_2$ electrolytes

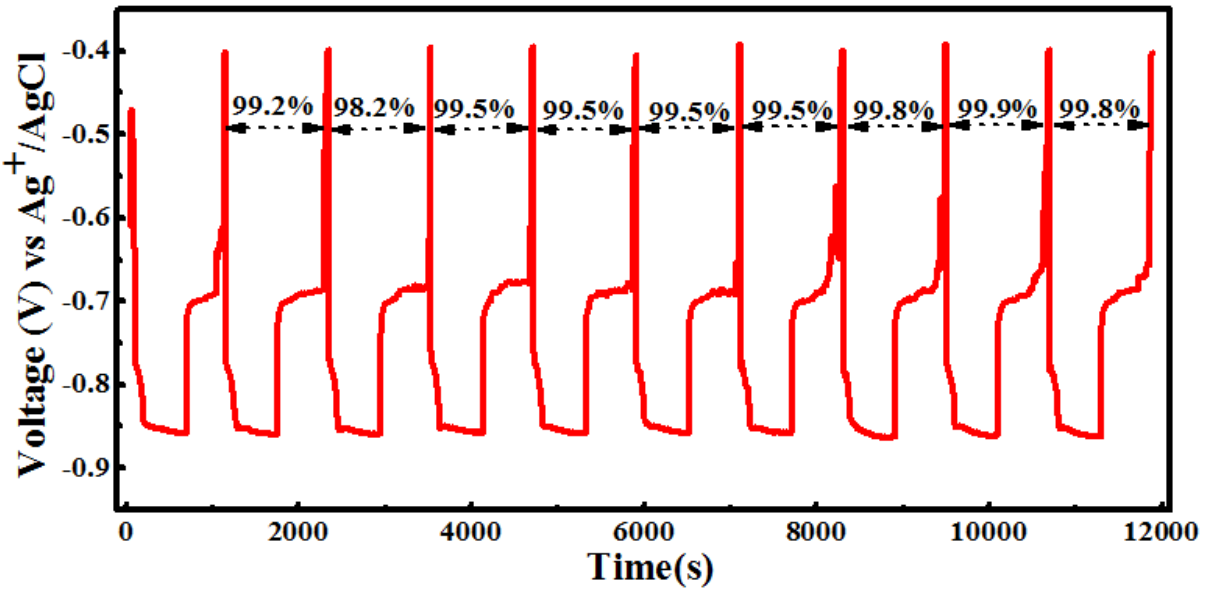

Figure S3. The voltage profiles of Zn plating/stripping on a Pt working electrode at 1 mA/cm^2 in the HCZE (1 m $Zn(TFSI)_2$+20 m LiTFSI) during the first 10 cycles.

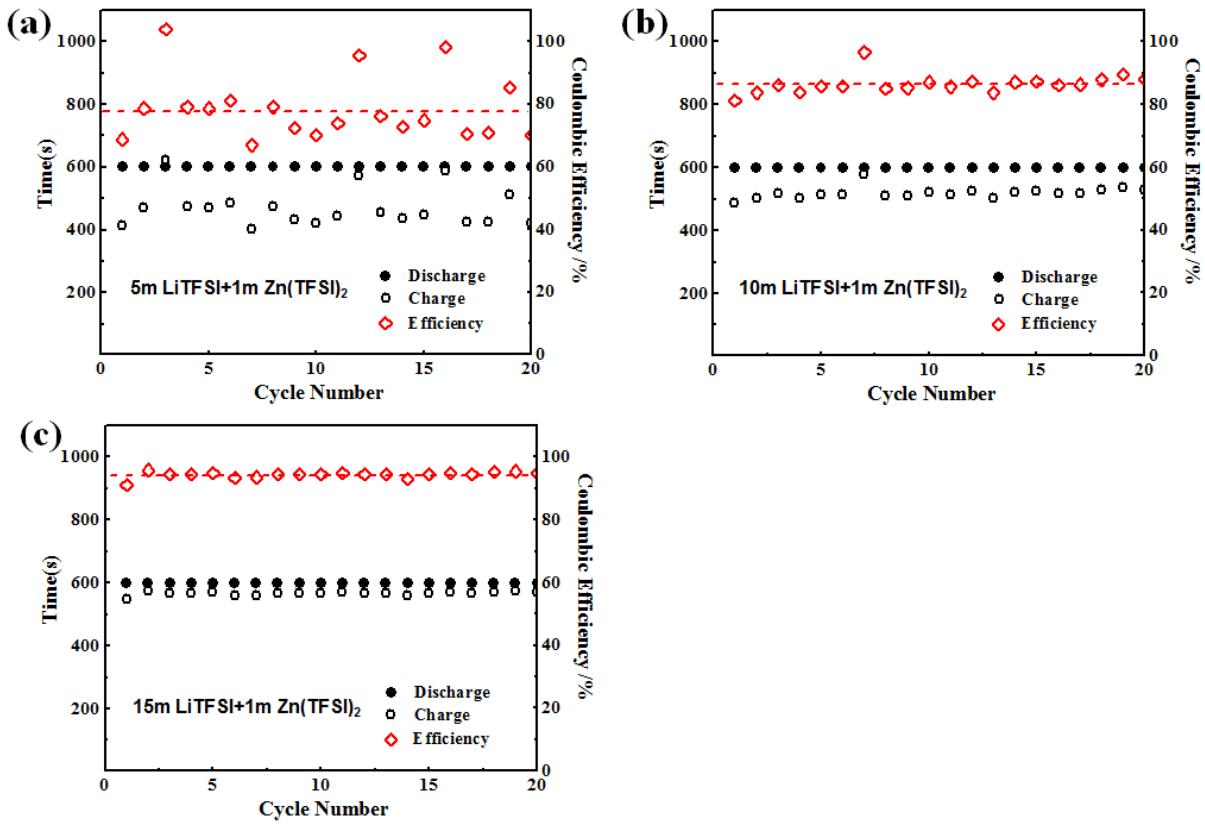

Figure S4. CEs of Zn metal plating/stripping on a Pt working electrode in the electrolytes with different LiTFSI concentrations at 1 mA/cm^2.

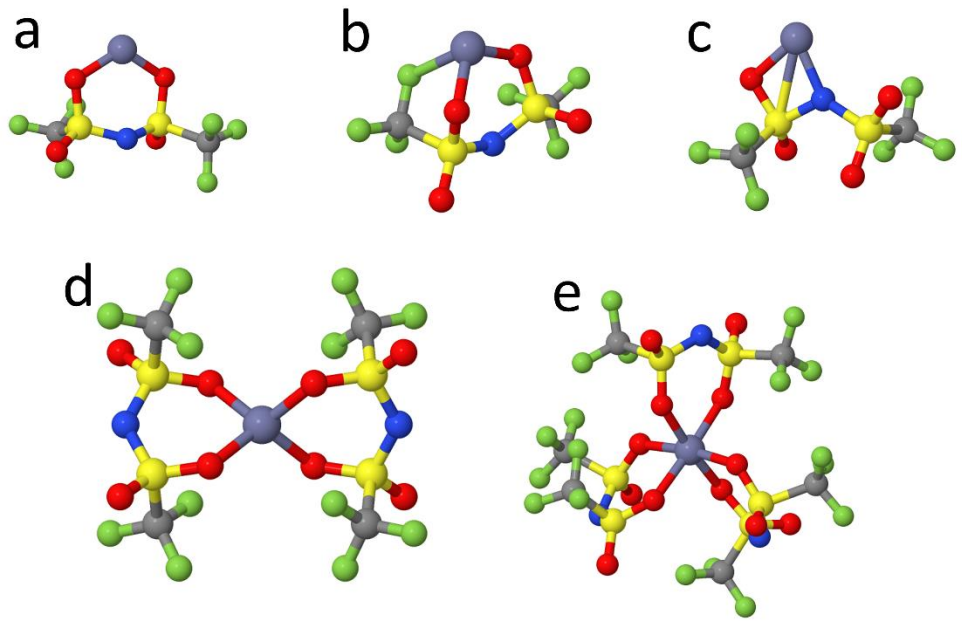

Figure S5. Optimized geometries of $Zn^{2+}(TFSI^-)_m$ clusters m=1,2,3 in gas-phase from M05-2X/6=311+G(2d2f) DFT calculations.

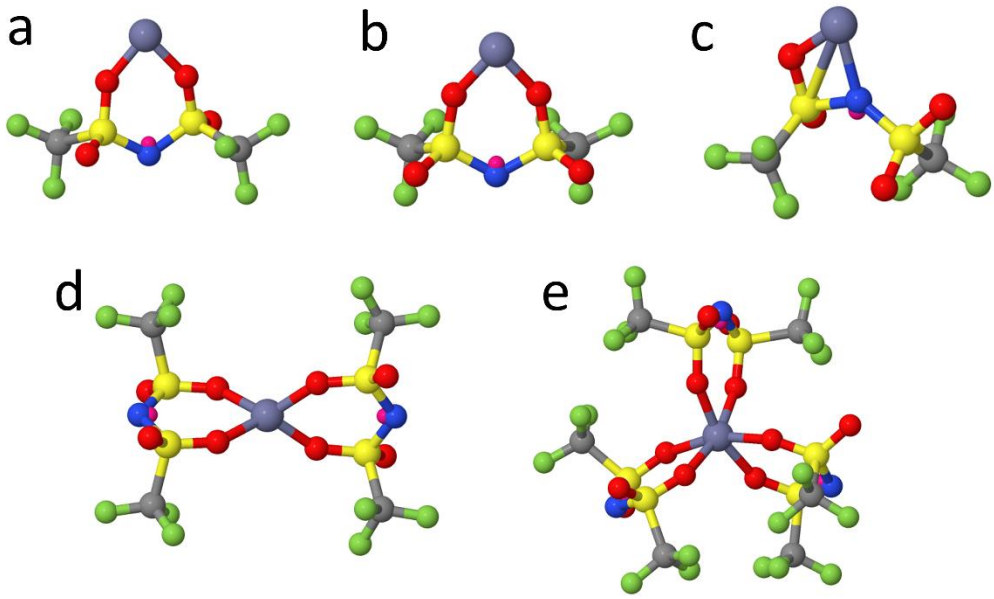

Figure S6. Optimized geometries of $Zn^{2+}(TFSI^-)_m$ clusters m=1,2,3 in gas-phase from molecular mechanics calculations utilizing developed force field.

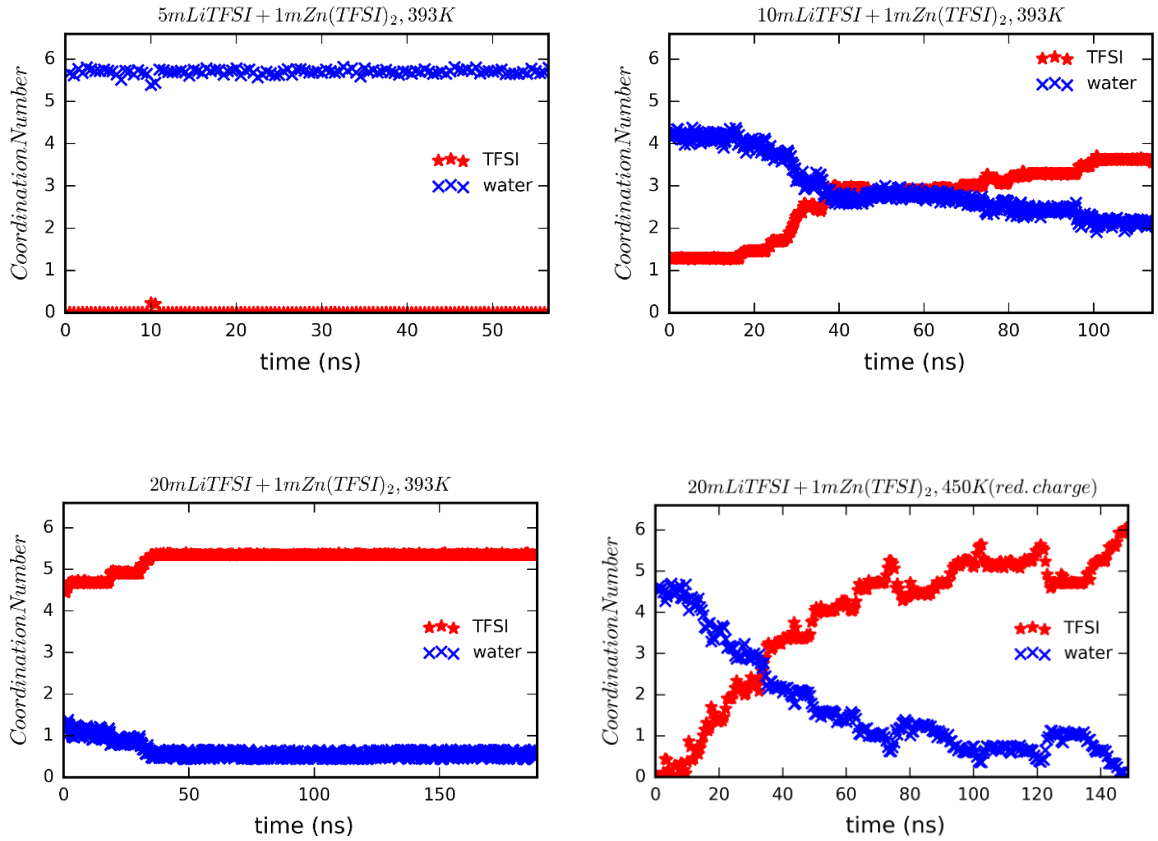

Figure S7. A representative evolution of the composition of the Zn^{2+} coordination shell during MD simulations at 393 K and 450 K showing the numbers for water and $TFSI^-$ oxygens within 2.8 Å of Zn^{2+}.

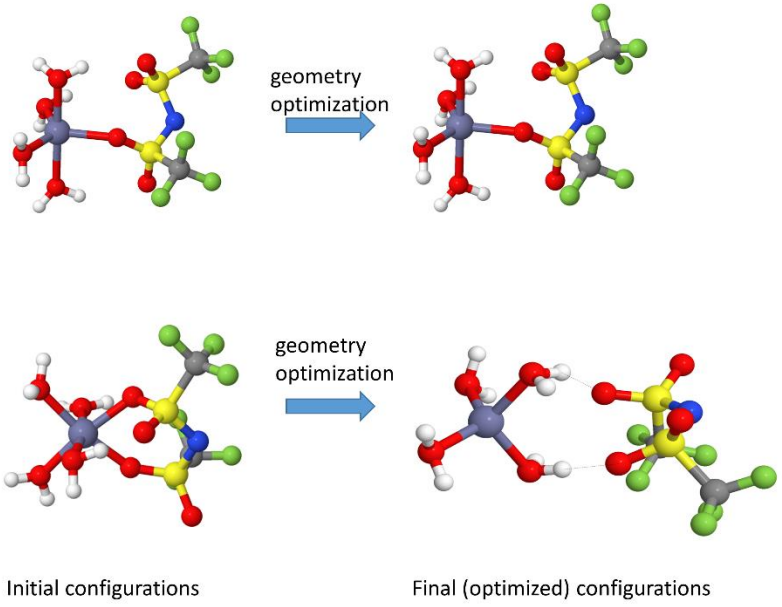

Figure S8. The initial and final (optimized) geometries of $Zn(TFSI)(H_2O)_4$ surrounded by SMD(water) implicit solvent from M05-2X/6-311+G(2d,2p) DFT calculations.

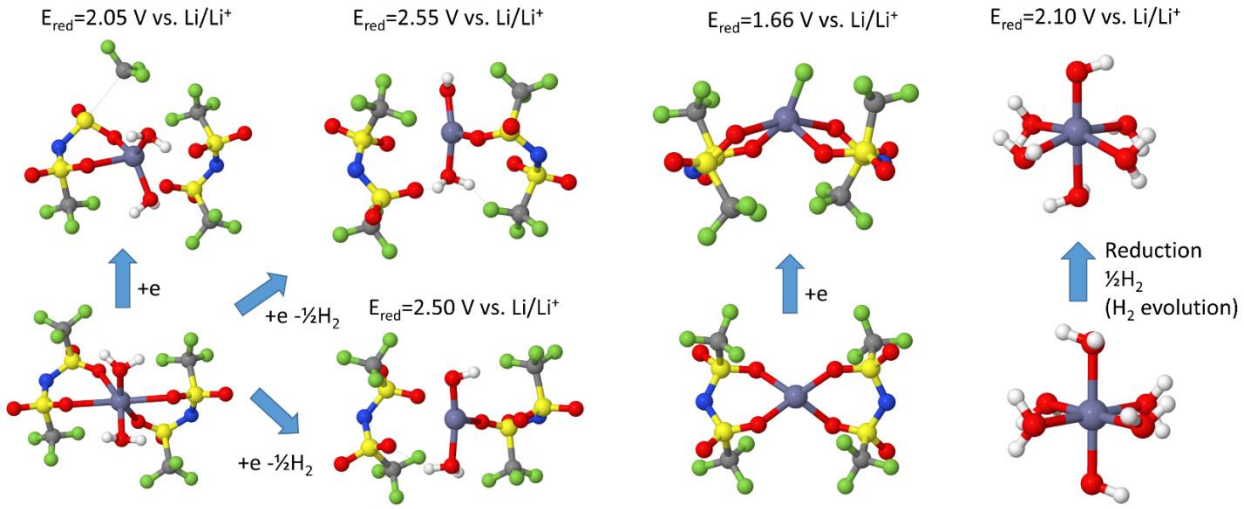

Figure S9. The reduction potential (E_{red} vs. Li/Li^+) from DFT calculations using M05-2X/6-311+G(2d,2p) with SMD(water) implicit solvation model. H_2 evolution occurs at higher potentials (~2.55 V vs. Li/Li^+) than S-F bond breaking or ZnF formation, thus when water is present in the Zn first solvation shell H_2 evolution is expected to occur first as anode potential is descreased during cycling.

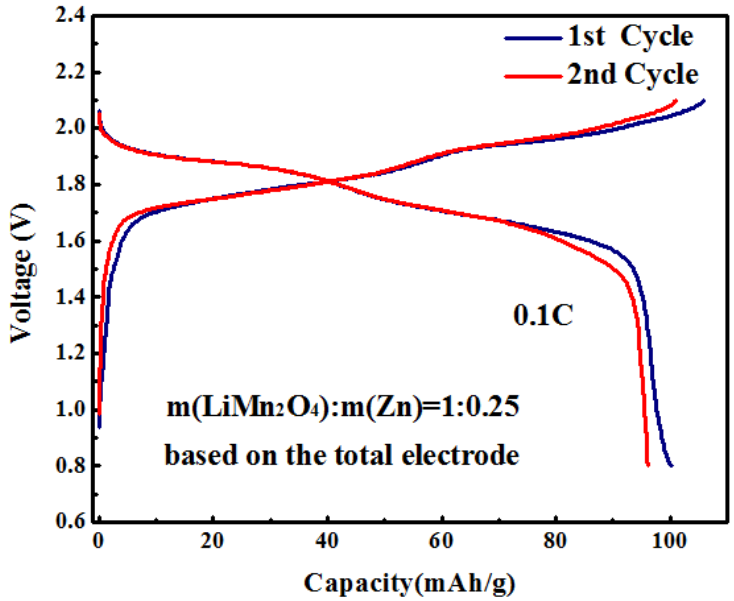

Figure S10. The typical voltage profile of $Zn/LiMn_2O_4$ full cell in the HCZE (1 m $Zn(TFSI)_2$+20 m LiTFSI)at 0.2 C (Zn-$LiMn_2O_4$ mass ratio 0.25:1).

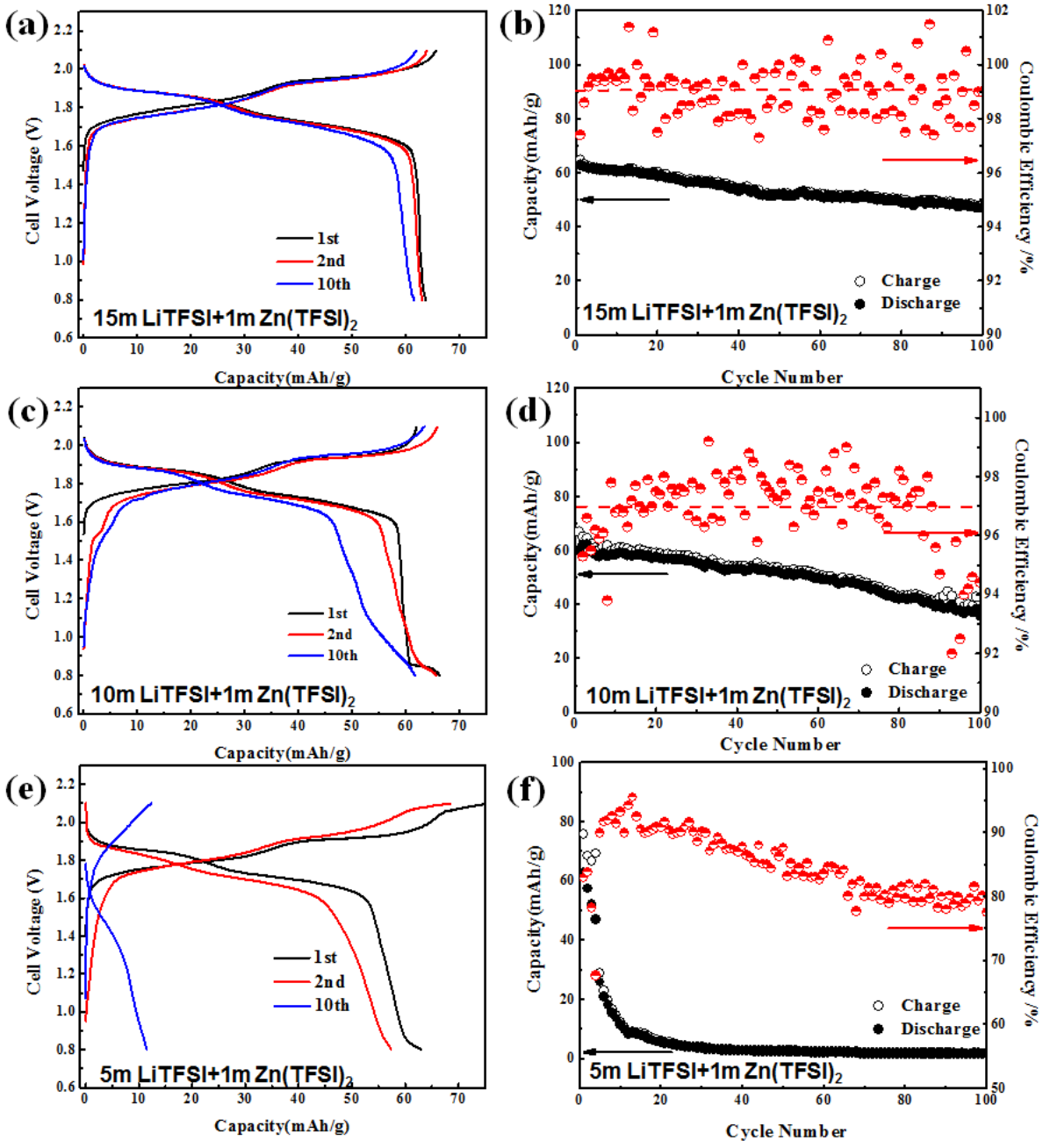

Figure S11. (a) The typical voltage profile and (b) the cycling stability and coulombic efficiency of the Zn/$LiMn_2O_4$ full cell in 15 m LiTFSI + 1 m $Zn(TFSI)_2$ solution at 0.2 C; (c)The typical voltage profile and (d) the cycling stability and coulombic efficiency of the Zn/$LiMn_2O_4$ full cell in 10 m LiTFSI + 1 m $Zn(TFSI)_2$ at 0.2 C; (e) The typical voltage profile and (f) the cycling stability and coulombic efficiency of the Zn/$LiMn_2O_4$ full cell in 5 m LiTFSI + 1 m $Zn(TFSI)_2$ solution at 0.2 C.

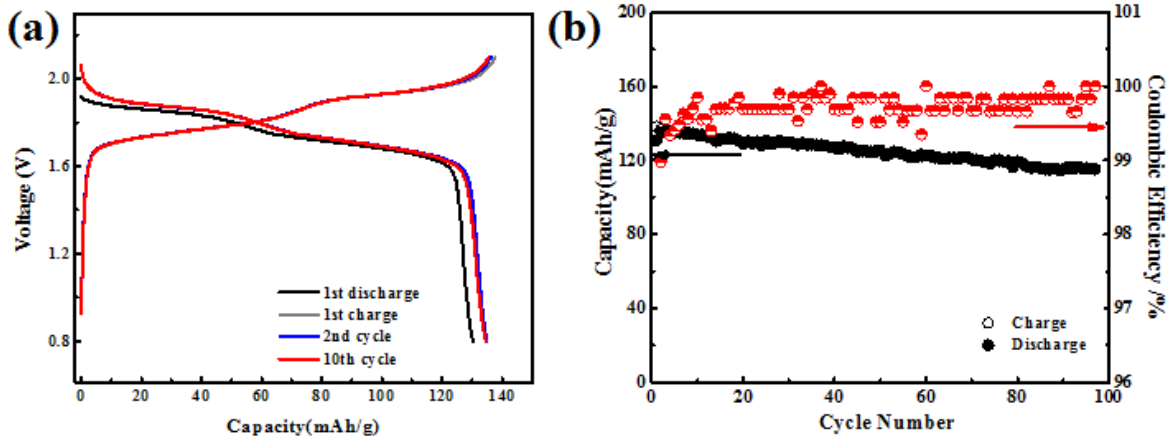

Figure S12. (a) The typical voltage profile and (b) the cycling stability and coulombic efficiency of the Zn/MnO_2 (delithiated $LiMn_2O_4$) full cell in the 0.2 m $Zn(TFSI)_2$+21 m LiTFSI electrolyte at 0.2 C.

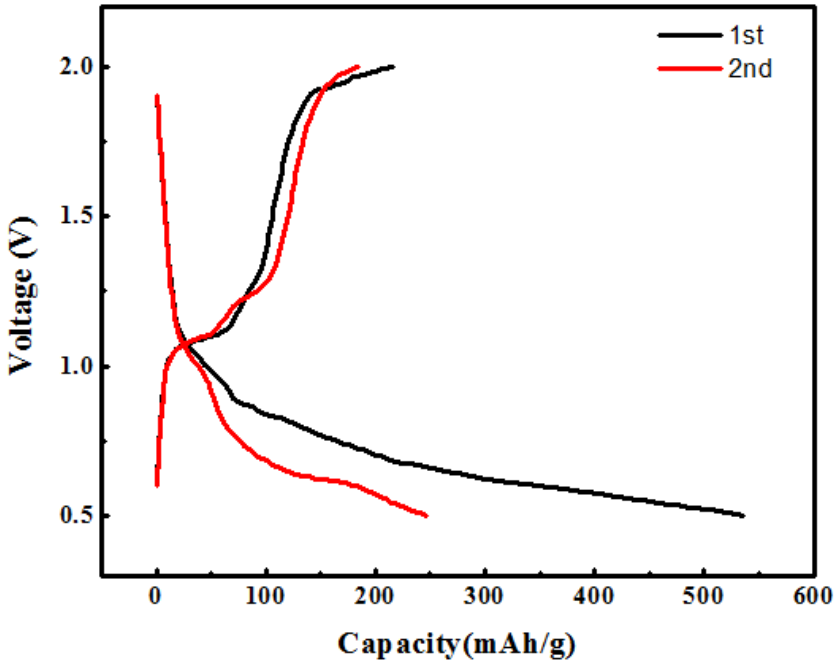

Figure S13. The typical full range voltage profile of Zn/O_2 batteries in the HCZE (1 m $Zn(TFSI)_2$+20 m LiTFSI) using only carbon paper as cathode at constant current of 50 mA/g between 0.5 V-2.0 V(based on the typical mass loading of super-P).

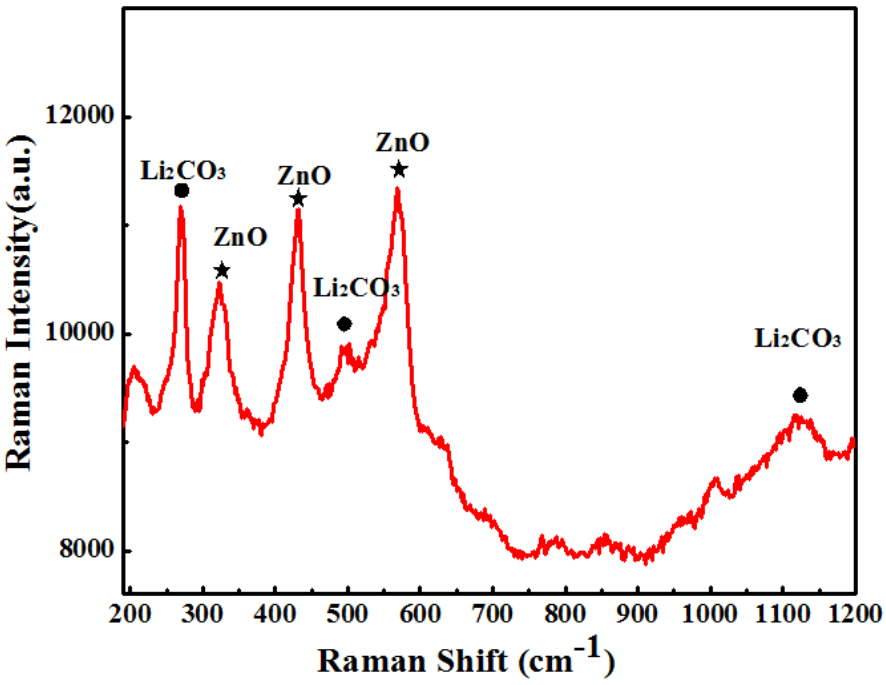

Figure S14. Raman spectrum of the cycled cathode at the discharge state of the Zn/O_2 cell.

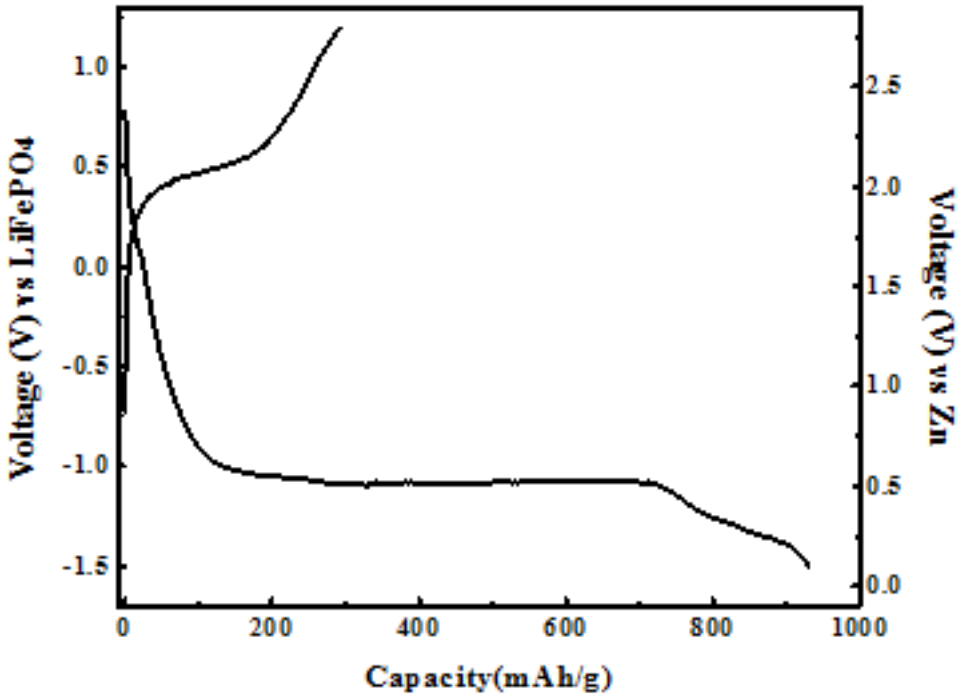

Figure S15. The typical full range voltage profile of $LiFePO_4/O_2$ batteries in the water-in-salt electrolyte using 70 wt.% super P as cathode at constant current of 50 mA/g between -1.5 V-1.2 V. The voltage was converted to Zn for convenience. Excessive $LiFePO_4$ was used here.

As shown in Figure S15, during the first discharging, Li-ions will be leached out from the $LiFePO_4$ and the Li-ions will react with the air electrode. However, the first discharging potential was much lower than that observed in the Zn/O_2 system. Besides that, the discharge capacity is only ¼ of Zn/O2 system. During the charging process, only 34% of the discharge capacity was delivered at a high voltage (higher than 2.0 V vs Zn). The overpotential is significantly higher than that of the Zn/O_2 system, indicating slower reaction kinetics.

Since the Zn-ion-free system shows much lower capacity, lower CE, higher overpotential and slower kinetics, we can conclude here that Zn-ion reactions with the air electrode dominates the entire process while a very small portion of the Li-ion reaction could still happen.

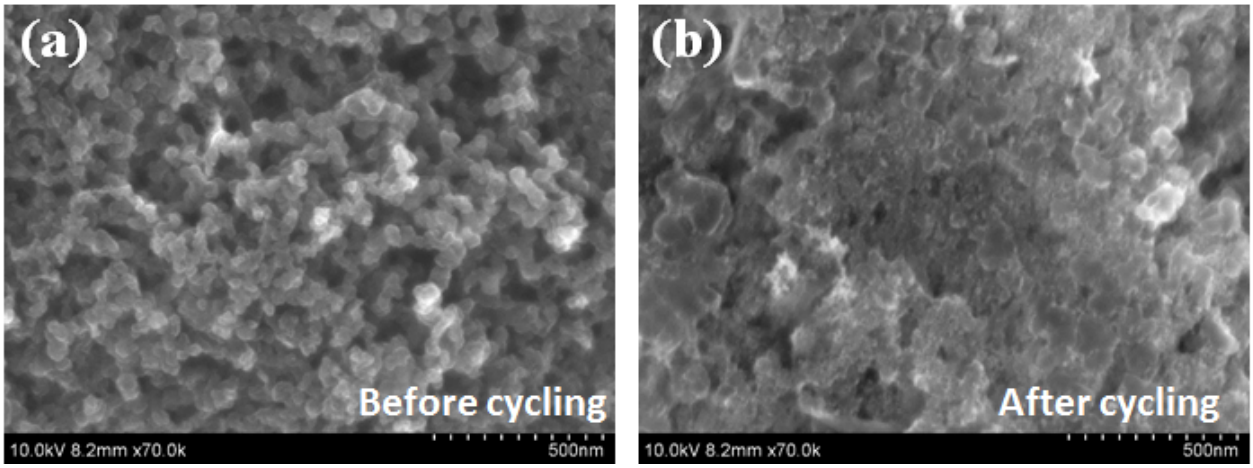

Figure S16. The SEM images for the O_2 cathodes before and after cycling.

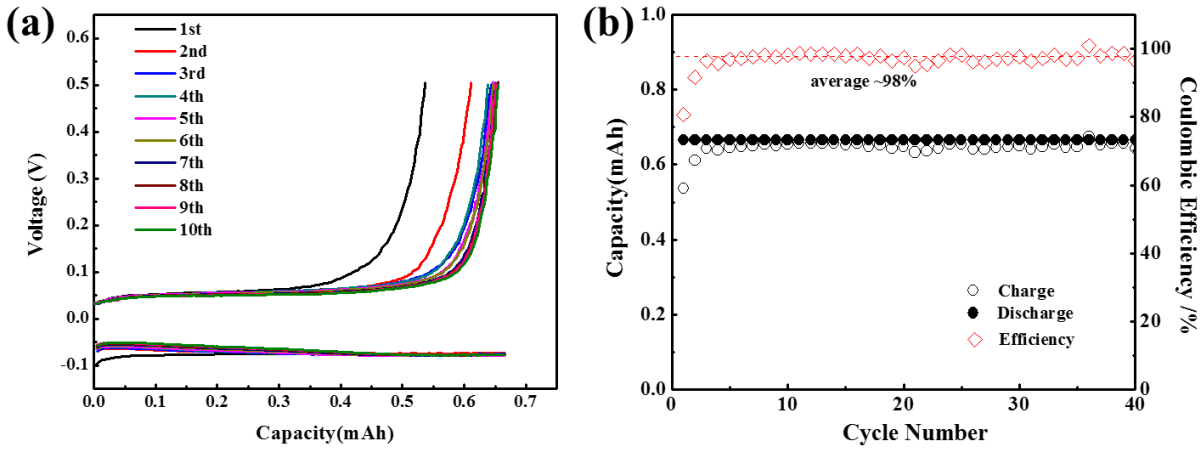

Figure S17. (a) The voltage profiles of Ti/Zn coin cell in the first 10 cycles during the Zn metal plating/stripping on a Ti working electrode at 1 mA/cm^2 in the 0.5 m $Zn(OTf)_2$+18 m $NaClO_4$ electrolyte. ($Zn(OTf)_2$, Zinc trifluoromethanesulfonate); (b) The corresponding CE of Zn metal plating/stripping on a Ti working electrode in the 0.5 m $Zn(OTf)_2$+18 m $NaClO_4$ electrolyte.

Reference

1 Borodin, O. Polarizable Force Field Development and Molecular Dynamics Simulations of Ionic Liquids. *J. Phys. Chem. B* **113**, 11463-11478(2009).

2 Asthagiri, D., Pratt, L. R., Paulaitis, M. E. & Rempe, S. B. Hydration Structure and Free Energy of Biomolecularly Specific Aqueous Dications, Including Zn2+ and First Transition Row Metals. *J. Am. Chem. Soc.* **126**, 1285-1289 (2004).

3 Marcus, Y. Effect of Ions on the Structure of Water: Structure Making and Breaking. *Chem. Rev.* **109**, 1346–1370 (2009).

4 Borodin, O. in T. R., Jow, K. Xu., O. Borodin & M, Ue (eds) *Electrolytes for Lithium and Lithium-Ion Batteries*. 371–401 (*Modern Aspects of Electrochemistry* Vol. 58, Springer, New York, 2014).